The Contribution of BeiDou-3 Binary Offset Carrier Signals to Single Point Positioning

Robert S.B. Galatiya SUYA, Yung-Tsang CHEN, Chiew-Foong KWONG, Penghe ZHANG, China, Craig Matthew HANCOCK, United Kingdom

Key words: BeiDou-3 BOC Signals, SNR, DOP, SPP, Positioning performance

SUMMARY

Aimed at providing first-class positioning, navigation, timing (PNT) services, the People's Republic of China successfully completed the commissioning of its modernised satellites with a BeiDou Navigation Satellite System (BDS)-3 Geostationary Earth Orbit (GEO) satellite in June 2020. As of December 2020, BDS has 49 nominal satellites in a constellation of which 44 are included in the operational orbital constellation and the remaining 5 are still in-orbit validation. Currently, BDS-3 satellites broadcast Binary Offset Carrier (BOC) signal frequencies (B1-C and B2a+b) with a completely unique modulation scheme to the other BDS-3 modernised signals (B2a and B2b) and the legacy B1I, B2I, and B3I (BDS-2) signals. With the multi-constellation and multi-frequency BDS signals, it is imperative to establish the current performance of the BDS modernised signals. Thus, in this paper, a comprehensive investigation of BDS is undertaken in terms of multipath; signal-to-noise ratio (SNR); the visible number of satellites; dilution of precision (DOP), and single point positioning (SPP). The investigation is based on 30 days datasets spanning from the day of the year (DOY) 153 to 182 in 2020 from 19 Multi-Global Navigation Satellite System (GNSS) Experiment (MGEX) tracking stations. The experimental results show that the modernised signals have more significantly reduced multipath errors than the legacy signals. For all the broadcast signals, the SNR is noticeably at least 42 dBHz. For both BDS-2 and BDS-3, at least 8 satellites are visible in each navigation system and their fusion pegs the average number of visible satellites to 15 thereby making DOP to improve from 4.8 to 2.5 by 48%. Based on the selected stations, the SPP performance of BOC signals only is more than 3 m in all three dimensions. The SPP performance is better than 0.78m, 0.51m, and 1.74m in the north, east, and vertical components, respectively. This indicates an average improvement of about 53%, 73%, and 61% in the north, east, and vertical dimensions, respectively. Upon the inclusion of the in-orbit validation BDS satellites in the operational orbital constellation, the overall SPP accuracy is likely going to improve and further extend the GNSS performance indicators.

The Contribution of BeiDou-3 Binary Offset Carrier Signals to Single Point Positioning

Robert S.B. Galatiya SUYA, Yung-Tsang CHEN, Chiew-Foong KWONG, Penghe ZHANG, China, Craig Matthew HANCOCK, United Kingdom

INTRODUCTION

The People's Republic of China's 54th satellite, a BDS-3 geostationary orbit (GEO) satellite, started rendering positioning navigation and timing (PNT) services in early June 2020(CSNO, 2020a). Belonging to the same GEO orbit is a 55th satellite which was successfully launched from Xichang Satellite Launch Center in Sichuan Province on July 23, 2020 (CSNO, 2020c). The former and latter BDS-3 GEO satellites are assigned pseudorandom noise (PRN) codes of PRN60 and PRN61, respectively. Coupled with the launches of modernised satellites made earlier in 2020, as indicated by the CSNO (2020b), BDS is a multi-constellation GNSS with a total satellites in constellation of 49 of which 44 are incorporated in the operational orbital constellation and only 5 are still in the testing phase.

In addition to the multiple satellites, both BDS-2 and BDS-3 satellites have multi-frequency broadcasting capability. The BDS-2 satellites transmit six navigation signals in three different frequency bands (B1-I, B2I, and B3I) of which B1I and B2I are equivalent to E5B of Galileo (Lu, Li, Yao, & Cui, 2019). The in-phase (I) and quadrature (Q) components are used to modulate the carrier frequency using a ranging code chip rate of either 2.046 or 10.23 Megachips per second (Mchip/s). The signal modulation scheme for BDS-2 B1I and B2I signals is different from that of B3I in that, the former is modulated with Quadrature Phase-Shift Keying (QPSK) whereas the latter is modulated using Binary Phase-Shift Keying (BPSK).

Table 0.1: Navigation signals for BDS-2 and BDS-3 satellites (CSNO, 2019).

Constellation	Band	Frequency [MHz]	Wavelength [cm]	Chip rate [Mcps]	Modulation
BDS-2	B1I	1561.098	19.20	2.046	BPSK
	B2I	1207.14	24.83	2.046/10.23	BPSK
	B3I	1268.52	23.63	10.23	BPSK
BDS-3	B1I	1561.098	19.20	2.046	BPSK
	B1-C	1575.42	19.03	1.023/2.046	QMBOC
	B2a	1176.45	25.48	10.23	QPSK
	B2b	1207.14	24.83	10.23	QPSK
	B2a+b	1191.795	25.15	15/10	ACE-BOC
	B3I	1268.52	23.63	10.23	BPSK

Unlike BDS-2, the modernised BDS-3 satellites broadcast six public service signals namely B1I, B3I, B2a+b, B2a, B2b, and B1-C. The BDS-3 B1I uses a different modulation mode

(BPSK) to its counterpart BDS-2 B1I signal. The modernized signal B2a+b utilizes the asymmetric constant envelope binary offset carrier (ACE-BOC). More details about the properties of the ACE-BOC modulation scheme can be found in Yao, Zhang, and Lu (2016). The rest of the BDS-3 signals employ BPSK modulation with B1-C signal utilizing Quadrature Multiplexed Binary Offset Carrier (QMBOC) as an additional modulation mode. Table 1.1 outlines an overview of the signal structure for BDS-2 and BDS-3. To enhance signal compatibility with other Global Navigation Satellite System (GNSS), BI-C is interoperable with GPS L1C signal (CNSO, 2017).

Alongside other GNSS, the BDS satellites are being used to augment Android three-dimensional (3D) maps for positioning in cities (Diggelen, 2020). In the transportation industry, the BDS signals are being used on more than 6 million vehicles in China (CGTN, 2020). BDS also presents exciting potential for use in the global civil aviation applications (Murfin, 2020; Ying & Jun, 2020); port dispatching in Pakistan (XinhuaNet, 2020); land surface categorization in advanced remote sensing (Yang et al., 2019) and in intelligent agriculture to facilitate the determination of soil temperature, humidity, and farm acreage (Meng, Yang, Wang, & Zhang, 2018). BDS is anticipated to extend its capability to quantum navigation, micro PNT, and, full source navigation in the near future (BNSS, 2020).

The SPP performance of BDS has been evaluated in different studies (Guo, Zhang, & Wang, 2015; Robustelli, Baiocchi, & Pugliano, 2019; Zhang, Chen, Gong, & Chen, 2020). Pei, Pan, & Liu (2017) evaluated combined SPP performance involing GPS and BDS constellations. A weighted dual-constellation was shown to have improved positioning accuarcy comapred with a GPS-only solution . In a similar study, Zhao, Cui, & Lu (2019) evaluated the SPP using both GPS and BDS satellites. The study employed both simulated and real signals in order to examine the positioning performance. In a multi-sensor integration application to determine receiver position, Wen & Hsu (2019) improved SPP with visible objects in the captured Light Detection and Ranging (LIDAR) by 35%. Luo *et al*, (2018) proposed a method to BDS SPP using base stations within a sparce network of receivers and the positinoning performance was improved by 83%, 72%, and 81% in North, East, and Up directions.

Despite the SPP research to evaluate the performance of BDS, the existing literature is still limited in the current performance of BDS modernised signals and their associated satellites. Thus, the robust characteristics of BDS-3 signal frequencies are a driving motivation to further evaluate the contribution of BDS new signals and satellites. In response there is a need to thoroughly characterise the code multipath for all the signals followed by the evaluation of SNR, and DOP before concentrating on SPP performance.

1 MATERIALS AND METHODS

1.1 Estimation of Parameters

1.1.1 Code Multipath

Code multipath has a significant contribution to code-based positioning such as SPP, precise point positioning (PPP), or navigation (Kaplan & Hegarty, 2017). Different signal frequencies implement similar or different modulation schemes which in turn demonstrate various levels of multipath. For both BDS-2 and BDS-3 constellation capable of broadcasting dual or more signals, the code multipath can be expressed as in Vaclavovic & Dousa (2016)

$$\left.\begin{aligned} MP_k &= P_k - \Phi_i - \beta\left(\Phi_i - \Phi_j\right) \\ &= P_k + \alpha\Phi_i + \beta\Phi_j \end{aligned}\right\} \quad [1.1]$$

$$\left.\begin{aligned} \alpha &= \frac{f_i^2\left(f_j^2 + f_k^2\right)}{f_k^2\left(f_i^2 - f_j^2\right)} \\ \beta &= \frac{f_j^2\left(f_i^2 + f_k^2\right)}{f_k^2\left(f_i^2 - f_j^2\right)} \end{aligned}\right\} \quad [1.2]$$

where denotes the MP_k pseudorange multipath; P_k and Φ_i denote the code and phase observations, respectively; f denotes the frequency; the subcripts k, i, and, j denote frequency indices; α and β denote the frequency combination scalars. The code multipath is thus computed as a quadratic mean or root mean square (RMS) value of a given sequence of epochs as (Kostelecký, Kostelecký, & Václavovic, 2017)

$$\left.RMS = \left(\frac{\sum_1^n v_i^2}{n}\right)^{\frac{1}{2}}\right\} \quad [1.3]$$

where n and v denote the number of continuous epochs and residuals, respectively.

1.1.2 Signal to Noise Ratio

GNSS receivers capable of tracking BDS signals are subject to receiving both line of sight (LOS) and non-line-of-sight (NLOS) signals. The NLOS are induced by the different reflecting objects within the receiver-satellite geometry. In other words, the NLOS are regarded as stochastic noise which impairs the performance of acquisition and tracking capabilities of a GNSS receiver. In a given receiver environment, the SNR is computed by the inherent receiver's tracking algorithm as a proportion between desired signal power and the background noise power in dBHz. Better SNR is characterised by higher magnitude of the the carrier noise power density ratio (C/N_0) which is, in turn, translated into better accuarcy (Strode & Groves, 2016). As indicated in Groves (2015), the SNR is described as good if higher than 42 dBHz for each tracked satellite.

1.1.3 Dilution of Precision

The performance of any GNSS has a strong correlation with the number of tracked satellites as well as satellite configuration which determine signal geometry.. As indicated in Kaplan & Hegarty (2017),for the horizontal GNSS positioning performance to be optimised, two factors are crucial. The first factor is that the signals from the low-elevation satellites should be available for the position fixing. The second factor is that the LOS vectors should be evenly distributed in the azimuth. On the other hand, the height performance is optimised when signals broadcast by satellites in the higher elevations are available.

Dilution of Precision (DOP) is used to quantify the influence of signal geometry on position quality. Optimal satellite arrangement in the sky leads to low DOP values. DOP is deduced from the diagonal elements of the cofactor matrix (Q). These elements are simply the variances that describe the North, East, Vertical (Up) and time DOP values, as expressed in [2.4], Leick et al. (2015):

$$\mathrm{Q} = \begin{bmatrix} q_N & & & \\ & q_E & & \\ & & q_U & \\ & & & q_\xi \end{bmatrix} \qquad [1.4]$$

where q_N, q_E, and q_U denote the DOP values for the North (N), East (E), Up (Up) dimensions, respectively; and q_ξ denotes the time DOP (TDOP) estimate. Depending on user requirements, the main diagonal entries are integrated to obtain the vertical dilusion of precision (VDOP); two-dimensional (2D) horizontal positioning (HDOP); three-dimensional (3D) position DOP (PDOP), and total geometry DOP (GDOP) expressed as

$$\left.\begin{aligned} VDOP &= (q_U^2)^{\frac{1}{2}} \\ HDOP &= (q_N^2 + q_E^2)^{\frac{1}{2}} \\ PDOP &= (q_N^2 + q_E^2 + q_U^2)^{\frac{1}{2}} \\ GDOP &= \left(q_N^2 + q_E^2 + q_U^2 + q_\xi^2\right)^{\frac{1}{2}} \end{aligned}\right\} \quad [1.5]$$

1.1.4 Single Point Positioning

Given the satellite positions and clock errors as computed from broadcast navigation message, SPP employs code observation data to solve the receiver positioning. The SPP solution is also known as the navigation solution and it can be executed using either dual- or multi-frequency code observations. For a given receiver i tracking satellites 1 to m, the SPP partial derivative matrix can be formulated as

$$\begin{bmatrix} p_i^1 \\ p_i^2 \\ \vdots \\ p_i^m \end{bmatrix} = \begin{bmatrix} \rho_i^1 + \Delta cdt_i^1 + I_i^1 + T_i^1 + M_i^1 \\ \rho_i^2 + \Delta cdt_i^2 + I_i^2 + T_i^2 + M_i^1 \\ \vdots \\ \rho_i^m + \Delta cdt_i^m + I_i^m + T_i^m + M_i^m \end{bmatrix} \quad [1.6]$$

with

$$\Delta cdt_i^1 = cdt_i - cdt^1 \quad [1.7]$$

where denotes the code measurement between the satellite (k) and receiver (i); Δcdt_i^1 denote the difference between the receiver (cdt_i) and satellite (cdt^k) clock errors, respectively; I_i^k and T_i^k denote the ionospheric and tropospheric delays, respectively, and M_i^k denotes the multipath.

Given that receiver i observes not less than four satellites, the SPP solution can be expressed as

$$\left.\begin{aligned} \boldsymbol{l} &= A.dx - V \\ dx &= (A^T W A)^{-1}(A^T W l) \\ \hat{\mathbf{x}} &= x_i^0 + dx \end{aligned}\right\} \quad [1.8]$$

with

$$\left.\begin{aligned}
&\boldsymbol{V} = [V_i^1\ V_i^2\ \ldots\ V_i^m]^T \\
&x_i^0 = [X_0^0\ Y_0^0\ Z_0^0\ cdt_i]^T \\
&dx = [V_X\ V_Y\ V_Z\ cdt_i]^T \\
&\boldsymbol{A} = \begin{bmatrix} -e_i^1 & -e_i^2 & \cdots & -e_i^m \\ 1 & 1 & \cdots & 1 \end{bmatrix}^T \\
&e_i^k = \left[\frac{(X_i^0 - X^k)}{(\rho_i^k)^0} \quad \frac{(Y_i^0 - Y^k)}{(\rho_i^k)^0} \quad \frac{(Z_i^0 - Z^k)}{(\rho_i^k)^0}\right] \\
&\boldsymbol{W} = diag(W_1, W_2, \cdots W_n) \\
&\boldsymbol{l} = \hat{\rho}_i^m - (\rho_i^m)^0 + cdt_i^0 - cdt^m + I_i^m + T_i^m + M_i^m
\end{aligned}\right\} \quad [1.9]$$

where $\boldsymbol{V}$ denotes the residual; x_i^0 denotes a vector of approximate coordinates ($X_0^0\ Y_0^0\ Z_0^0$) and receiver clock error; dx denotes the vector of corrections to the estimated values; $\boldsymbol{A}$ denotes the Jacobian matrix containing the LOS vectors (e_i^k); $\boldsymbol{W}$ denotes the weight matrix, and $\boldsymbol{l}$ denotes the least squares solution.

For the given number of satellites in view, the standard deviation of unit weight for a weighted adjustment ($\breve{\sigma}_0$) and its corresponding RMS error for the n^{th} unknown can be expressed as

$$\left.\begin{aligned}
&\breve{\sigma}_0 = [(V^T W V)/r]^{\frac{1}{2}} \\
&RMS_n = \breve{\sigma}_0 . [(A^T W A)^{-1}]^{\frac{1}{2}}
\end{aligned}\right\} \quad [1.10]$$

where r denotes the number of degrees of freedom.

1.2 Experimental Description

To thoroughly examine the contribution of BDS-3 BOC signals to SPP, the real BDS datasets from 19 MGEX stations (https://www.igs.org/) were employed. For these stations, 30 days datasets spanning from DOY 153 to 182 in 2020 were used. The geographical locations for the selcted stations are presented in Figure 2.1 and Table 2.1.

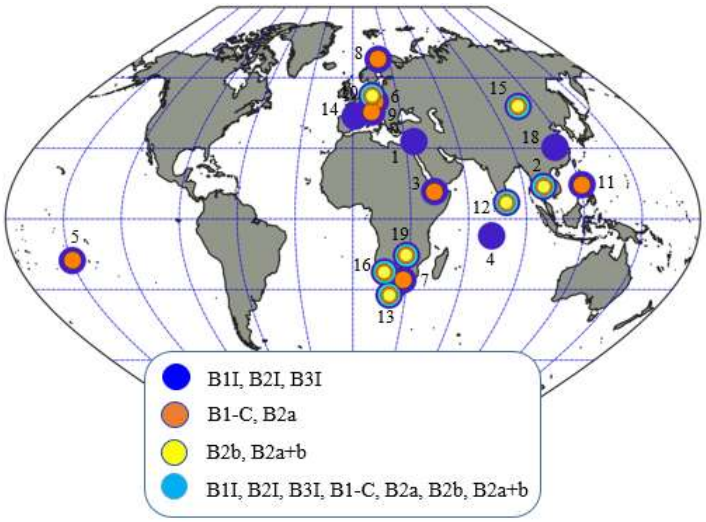

Figure 1.1: Geographical distribution of the selected MGEX stations.

Table 1.1: Station metadata.

SN	ID	Latitude	Longitude	Receiver Type	Antenna Type	Dome
1	bshm	32° 46' 44.4"	35° 01' 12.0"	JAVAD TRE_3 DELTA	TRM59800.00	SCIS
2	cusv	13° 44' 09.3"	100° 32' 02.1"	JAVAD TRE_3 DELTA	JAVRINGANT_DM	NONE
3	dgar	-08° 43' 49.1"	72° 22' 12.9"	SEPT POLARX5	TRM59800.00	NONE
4	djig	11° 31' 34.6"	42° 50' 49.4"	SEPT POLARX5	TRM59800.00	NONE
5	faa1	-18° 26' 40.9"	-150° 23' 08.5"	SEPT POLARX5	LEIAR25.R4	NONE
6	gop6	49° 54' 49.2"	14° 47' 08.2"	SEPT POLARX5	SEPCHOKE_B3E6	SPKE
7	harb	-26° 06' 46.9"	27° 42' 26.1"	SEPT POLARX5TR	TRM59800.00	NONE
8	kiru	67° 51' 26.5"	20° 58' 06.4"	SEPT POLARX5	SEPCHOKE_B3E6	SPKE
9	pado	45° 24' 40.1"	11° 53' 45.8"	SEPT POLARX5	SEPCHOKE_B3E6	SPKE
10	pots	52° 22' 45.5"	13° 03' 57.9"	JAVAD TRE_3	JAVRINGANT_G5T	NONE
11	ptgg	14° 32' 07.5"	121° 02' 28.6"	SEPT POLARX5	TRM59800.00	SCIS
12	sgoc	06° 53' 31.5"	79° 52' 27.1"	JAVAD TRE_3	JAVRINGANT_G5T	NONE
13	sutm	-33° 37' 06.8"	20° 48' 39.3"	JAVAD TRE_3	JAVRINGANT_G5T	NONE
14	tlse	43° 33' 38.5"	01° 28' 51.2"	TRIMBLE NETR9	TRM59800.00	NONE
15	ulab	47° 51' 54.2"	107° 03' 08.4"	JAVAD TRE_3	JAVRINGANT_G5T	NONE
16	wind	-23° 25' 30.3"	17° 05' 22.0"	JAVAD TRE_3	JAVRINGANT_G5T	NONE
17	wtzz	49° 08' 39.2"	12° 52' 44.0"	JAVAD TRE_3 DELTA	LEIAR25.R3	LEIT
18	wuhn	30° 31' 54.0"	114° 21' 26.1"	TRIMBLE NETR9	TRM59800.00C	ENCL
19	zamb	-16° 34' 28.1"	28° 18' 39.6"	JAVAD TRE_3 DELTA	AOAD/M_T	NONE

To process the datasets, an open source G-Nut/Anubis 2.3 software library was utilized. Developed at Geodetic Observatory Pecny (GOP, https://gnutsoftware.com/software/anubis/), G-Nut/Anubis is the C++ object-oriented command-line GNSS software whose free-version runs on Linux. Capable of handling both Receiver INdependent Exchange (RINEX) 2.x and RINEX 3.x (where 2.x and 3.x stand for the RINEX version), the G-Nut/Anubis free-program is mainly a GNSS quality-checking (QC) software with multi-fundamental functionalities including the determination of the signals; bands; satellites; azimuths; elevations; code

multipath; SNR; DOP, and SPP repeatability. Taking advantage of the multiple capabilities of the software, all the variables described in Section 2.1 were output from a single command based on the pre-defined standard Extensible Markup Language (XML) configuration file containing the station identities (ID) depicted in Table 2.1.

2 RESULTS AND DISCUSSIONS

2.1 Multipath

Using Equation [2.3], the RMS values for the BDS-2 and BDS-3 signals were estimated and their averaged solutions for the 30 days at each station are presented in Figure 3.1. As can be seen in the upper panel of Figure 3.1, multipath effects for BDS-2 are the highest (about 69 cm at BSHM station) and the lowest least (about 9.4 cm at CUSV station) at C2I signal and C6I signal, respectively, among the triple signals of C2I, C7I, and C6I for BDS-2. The BDS-2 RMS numerical values are summarised in Table 3.1.

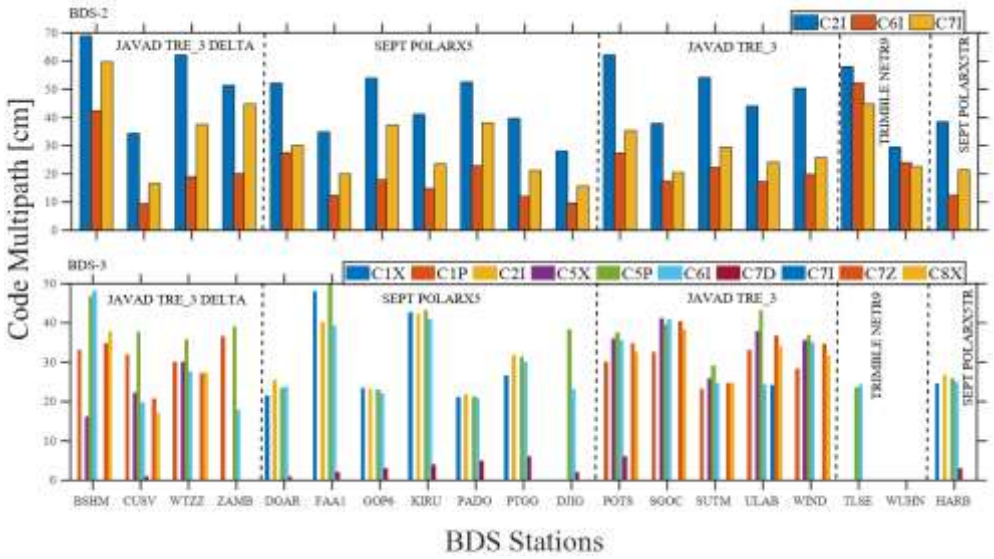

Figure 2.1: Code multipath comparison.

As for BDS-3 signals, it is evident from Figure 3.1 (lower panel) that the RMS value of the C7D signal outperformed all the other signals with multipath effects of less than 10 cm at all the stations. For the C7D signal, the minimum and maximum multipath effects of about 1 cm and 6 cm, respectively and an averaged RMS value of about 3 cm were achieved for the selected stations (Table 3.2). For both BDS-2 and BDS-3 (Figure 3.1), the multipath effects are different for the same receiver architecture installed in different locations. This is attributed to the fact that multipath is location-dependent such that different environments have unique sources of electromangnetic radiation that affect the GNSS signals (Atilaw, Cilliers, & Martinez, 2017).

Table 2.1: BDS-2 multipath statistics.

	C2I	C6I	C7I
Minimum [cm]	28.10	9.40	15.70
Maximum [cm]	69.00	52.20	59.80
Average [cm]	47.08	21.10	29.96

Table 2.2: BDS-3 multipath statistics.

	C1X	C1P	C2I	C5X	C5P	C6I	C7D	C7Z	C8X
Minimum [cm]	21.20	23.20	21.90	16.10	21.40	17.90	1.00	20.70	17.20
Maximum [cm]	48.10	36.50	42.40	41.20	49.80	48.20	6.00	40.50	38.40
Average [cm]	29.71	31.04	30.29	30.66	34.81	29.10	3.30	31.79	30.51

2.2 SNR

The SNR for all the BDS-2 and BDS-3 frequencies were estimated and their averaged results for the selcted days are plotted in Figure 3.2. In Figure 3.2, the numbers 1 to 4 denote JAVAD TRE_3 DELTA; SEPT POLARX5; JAVAD TRE_3; TRIMBLE NETR9, and SEPT POLARX5TR, respectively. For the five different receiver types in Figure 3.2, 92.16% of the estimated SNR are above 42 dBHz. In an environment less susceptible to interference, an ideal GNSS antenna should output a SNR of not less than 42 dBHz (Groves, 2015).

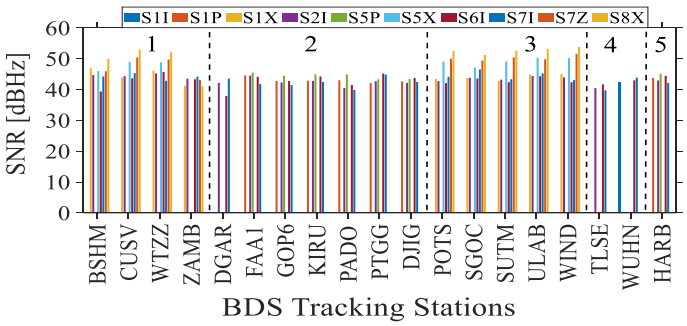

Figure 2.2: SNR time series for all the selected stations.

Since SNR quantifies signal strength in the presence of noise (Hetet & Langley, 2000), then the estimated SNR for each frequency is within the acceptable limits (above 42 dBHz) to offer positioning performance.. To be within the permissible tolerance, the SNR values should approximately range from 30 to 40 dBHz at elevations less than 60º and 50 to 55 dBHz at higher elevations, such as elevations above 60º (Estey & Wier, 2013). To demonstrate the strength of the signals, the SNR values for the ZAMB station are plotted against the elevation angle in Figure 3.3 on four different days (DOY 158, 165, 172, and 179). As can be evidenced in Figure 3.3, all the SNR time series are noisier at low elevation angles than at higher angles as would be expected. The higher noise at low elevation angles may be attributed to multipath effects.

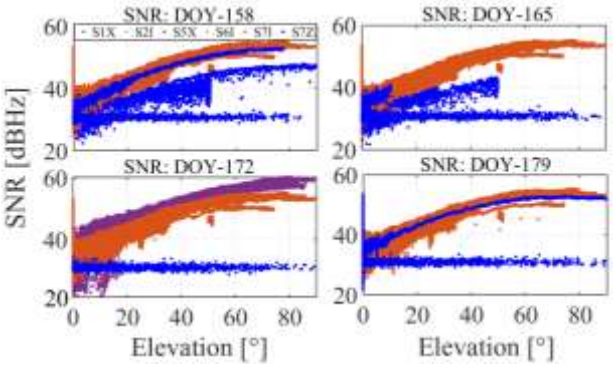

Figure 2.3: SNR with respect to elevation at ZAMB on DOY 158, 165, 172 and 179.

2.3 Number of Satellites and DOP

The number of satellites in view and their geometry determine the quality of PNT estimates. The satellite configuration varies with time when the satellite rises; moves across the sky; and then disappears below the horizon. To obtain the PNT estimates in 3D, at least four satellites need to be in view. The averaged number of satellites in view for BDS-2, BDS-3, and a combination of BDS-2 and BDS-3 were estimated and are depicted in Figure 3.4. From Figure 3.4, it can be seen that the combined number of satellites (BDS-2 and BDS-3, yellow bars in the left panel) is higher than that of the individual navigation systems for all the stations. Combining BDS-2 and BDS-3 navigation systems improves the visible number of satellites for each station by the percentages depicted in Figure 3.4 (right panel). Moreover, at least 19 satellites can be tracked at each station in the combined system. Table 3.3 summarises the statistics for the averaged number of satellites.

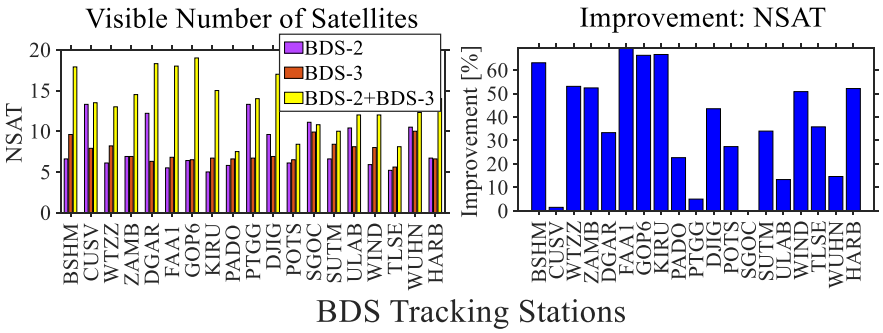

Figure 2.4: Averaged number of satellites and improvement in the visible number of satellites.

Table 2.3: Averaged number of satellites.

	BDS-2	BDS-3	BDS-2+BDS-3	Improvement [%]
Min	5	6	7	2
Max	13	10	19	69
Average	8	7	14	38

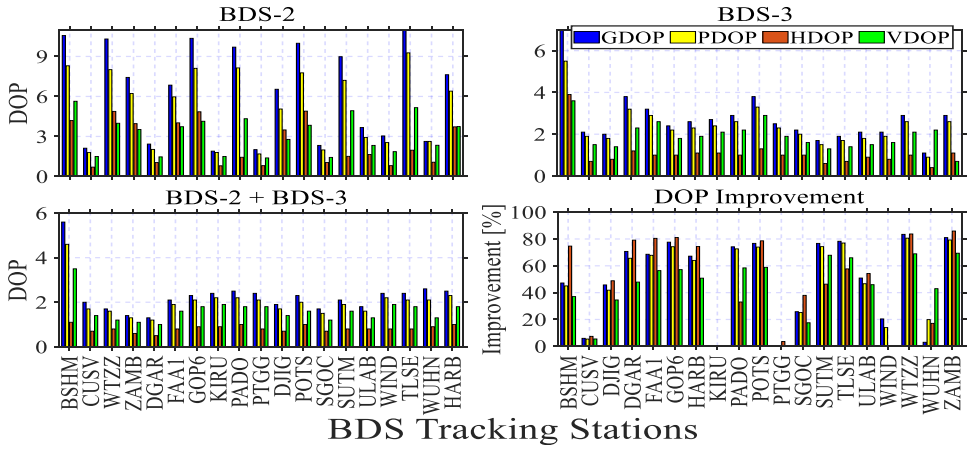

Figure 2.5: Averaged DOP for the selected stations.

Corresponding to the number of satellites (in Figure 3.4) are the DOP values for BDS-2, BDS-3, and the integrated systems of BDS-2 and BDS-3 depicted in Figure 3.5 and Table 3.4. The DOP values improve with respect to the increase in the number of satellites. For example, Table 3.4 demonstrates a decrease in BDS-2+BDS-3 DOP with respect to both BDS-2 and BDS-3 individual systems indicating better precision. For all the stations, the averaged improvement in the maximum GDOP, PDOP, HDOP, and VDOP values as a result of adding BDS-3 to BDS-2 satellites are about 83%, 80%, 66%, and 69%, respectively (Table 3.4).

Table 2.4: Averaged DOP statistics.

	BDS-2				BDS-3				BDS-2 + BDS-3				Improvement [%]			
	GDOP	PDOP	HDOP	VDOP	GDOP	PDOP	HDOP	VDOP	GDOP	PDOP	HDOP	VDOP	GDOP	PDOP	HDOP	VDOP
Min	1.90	1.69	0.70	1.39	1.05	0.91	0.41	0.71	1.32	1.18	0.53	0.96	3.01	5.41	0.35	5.47
Max	11.00	9.27	4.90	5.64	6.96	5.48	3.92	3.55	5.58	4.56	1.06	3.55	83.47	80.63	85.94	69.41
Average	6.29	5.15	2.47	3.14	2.72	2.39	1.08	1.93	2.29	2.01	0.81	1.63	56.09	54.56	52.49	49.08

2.4 Single Point Positioning

The SPP for each station was performed using the models derived in Section 2.1.4. The RMS errors for the selected days and stations were estimated using equation [2.10]. The averaged RMS errors are for each station are presented in Figure 3.6 and their corresponding statistics are summarised in Table 3.5. For BDS-2, the mean RMS errors are 1.54 m, 4.16 m, and 4.97 m, whereas those of BDS-3 are 0.88 m, 0.89 m, and 2.05 m, in North(N), East(E), and Up (U), respectively (Table 3.5).

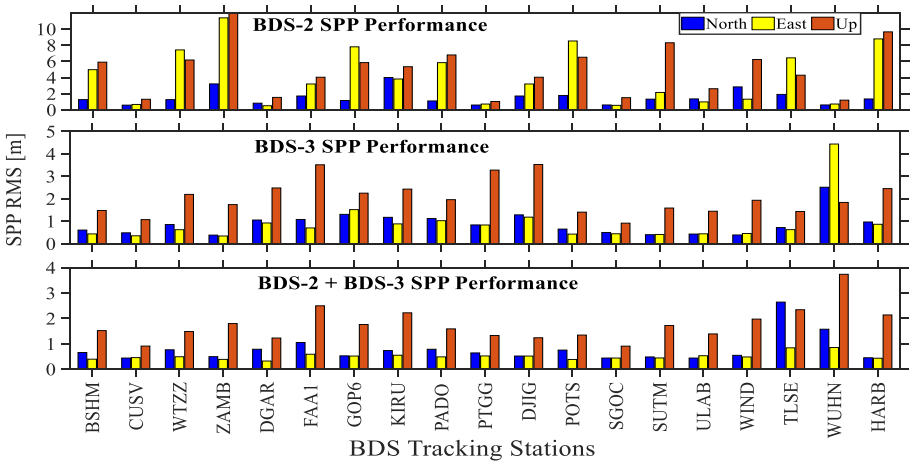

Figure 2.6: BDS SPP performance.

For the selected days, the combined processing of B1C and B2a+b signals for BDS-3 satellites result in an averaged SPP performance of 3.40 m, 3.75 m, and 8.31 m in N, E, and U dimensions, respectively. Figure 3.7 depicts the results for the stations with B1C and B2a+b capability. As can be evidenced from Figure 3.7, about 83% of the stations have SPP performance of less than 5 m in both N and E dimensions. Similarly, about 83% of the stations have an SPP performance of at least 10 m in height. Table 3.5 summarises the SPP performance statistics for the stations with B1C and B2a+b tracking capability.

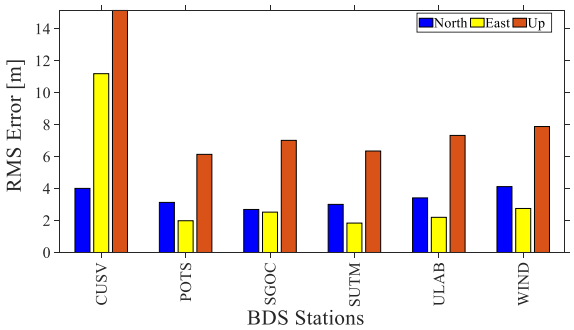

Figure 2.7: SPP performance for B1C and B2a+b.

Table 2.5: SPP performance statistics for stations with B1C and B2a+b tracking capability.

Station	North [m]	East [m]	Up [m]
Min	2.69	1.84	6.14
Max	4.12	11.19	15.15
Average	3.4	3.75	8.31

The integrated processing of BDS-2 and BDS-3 leads to an SPP performance of 0.72 m, 0.51 m, and 1.74 m in N, E, U dimensions, respectively. As averaged from all the stations, the BDS-2 and BDS-3 combined processing improves the overall SPP performance in N, E, and U by about 53%, 73%, and 61%, respectively (Table 3.5). As opposed to BDS-2+BDS-3 integrated processing (Figure 3.6), the averaged errors in all the three dimensions for the B1-C and B2a+b combined processing in Figure 3.7 are all above 3 m. This may be attributed to the reduced number of satellites with BOC signal tracking capability. On the other hand, the addition of GPS and Galileo to BDS observations only leads to an improvement of less than 25% in all the three dimensions of N (18.96%), E (23.66%), and U (20.42%). Figure 3.8 and Table 3.6 depict the comparison of SPP performance between BDS and other navigation systems.

Table 2.6: SPP performance statistics for BDS-2, BDS-3 and BDS-2+BDS-3.

Station	BDS-2 [m]			BDS-3 [m]			BDS-2 + BDS-3 [m]			Improvement [%]		
	N	E	U	N	E	U	N	E	U	N	E	U
Min	0.59	0.52	1.04	0.38	0.34	0.92	0.44	0.32	0.91	5.76	22.40	20.77
Max	4.01	11.39	11.96	2.52	4.44	3.53	2.64	0.85	3.74	84.65	96.60	84.98
Average	1.54	4.16	4.97	0.88	0.89	2.05	0.78	0.51	1.74	52.71	72.57	60.99

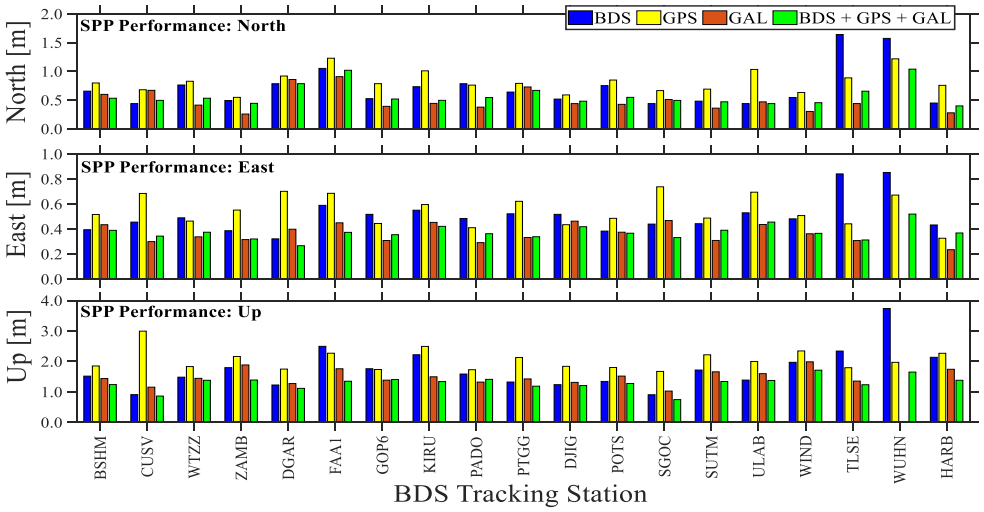

Figure 2.8: Comparison of SPP performance.

Table 2.7: BDS SPP performance statistics with respect to other navigation systems.

Station	BDS [m]			GPS [m]			GAL[m]			BDS + GPS + GAL[m]			Improvement [%]		
	N	E	U	N	E	U	N	E	U	N	E	U	N	E	U
Min	0.44	0.32	0.91	0.55	0.41	1.67	0.26	0.24	1.03	0.40	0.27	0.75	1.05	1.14	0.86
Max	2.64	0.85	3.74	1.23	5.33	2.99	0.91	0.47	1.99	1.04	0.52	1.71	75.18	62.85	55.81
Average	0.78	0.51	1.74	0.83	0.81	2.05	0.49	0.37	1.49	0.58	0.37	1.30	21.40	23.65	20.43

3 CONCLUSIONS

BDS is a multi-frequency and multi-constellation GNSS with a total satellites in constellation of 49 of which 44 are incorporated in the operational orbital constellation and only 5 are still in the testing phase. In addition to the BDS-2 legacy frequencies, the modernised BDS-3 satellites transmit signals with different modulation schemes. In this paper, the BDS signals were investigated in terms of code multipath; SNR; NSAT; DOP, and SPP using 30 days BDS datasets from 19 MGEX tracking stations. The results demonstrate that the modernised signals have fewer multipath effects than the legacy signals. The mean SNR for 92% of the selected stations is within the acceptable limit of at least 42 dBHz. For BDS-2+BDS-3, at least 19 satellites can be tracked at each station as opposed to 13 and 10 in BDS-2 and BDS-3, respectively thereby making GDOP improve by about 56%. Based on the selected stations, the SPP performance of BOC signals only is more than 3 m in all three dimensions. The combined BDS-2+BDS-3 SPP performance is better than 0.72 m, 0.51 m, and 1.74 m in the north, east, and vertical components, respectively. With respect to BDS-2 only processing, this indicates a convincing improvement of about 53%, 73%, and 61% in the north, east, and vertical dimensions, respectively. On the other hand, the addition of GPS and Galileo to BDS observations only leads to an improvement of less than 25% in all three dimensions. Thus, upon the inclusion of the in-orbit validation BDS satellites in the operational orbital constellation, the overall SPP accuracy is likely going to improve and further extend the GNSS performance indicators.

ACKNOWLEDGEMENTS

The authors extend their acknowledgments to both the International GNSS Service and Geodetic Observatory Pecny for access to the datasets and software, respectively. This work is supported by Ningbo Science and Technology Bureau under Commonweal Research Program with project code 2019C50017 and a research grant with project code A0060 from Ningbo Nottingham New Material Institute.

5 REFERENCES

Atilaw, T. Y., Cilliers, P., & Martinez, P. (2017). Azimuth-dependent elevation threshold (ADET) masks to reduce multipath errors in ionospheric studies using GNSS. *Advances in Space Research*. https://doi.org/10.1016/j.asr.2016.10.021

BNSS. (2020). Completion and Commissioning of the BeiDou Navigation Satellite System (BDS-3). Retrieved August 3, 2020, from BeiDou Navigation Satellite System (BNSS) website: http://en.beidou.gov.cn/WHATSNEWS/202008/t20200803_21013.html

CGTN. (2020). BeiDou navigation services applied to over 6 million vehicles in China: Transport Ministry. Retrieved June 23, 2020, from China Global Television Network

(CGTN) website: https://news.cgtn.com/news
CNSO. (2017). *BeiDou Navigation Satellite System Signal in space interface control document open service signal B2a (version 1.0)*. http://www.beidou.gov.cn/xt/gfxz
CSNO. (2020a). Beidou satellite navigation system 54th satellite officially provides service. Retrieved June 2, 2020, from China Satellite Navigation System Management Office Test Evaluation Research Center- Test and Assessment Research Center of China Satellite Navigation Office website: http://www.csno-tarc.cn/notice
CSNO. (2020b). Current position: Beidou system status- Constellation status. Retrieved January 12, 2021, from China Satellite Navigation System Management Office Test Evaluation Research Center Test and Assessment Research Center of China Satellite Navigation Office website: http://www.csno-tarc.cn/system/constellation
CSNO. (2020c). The last networked satellite of Beidou-3 system joins the network. Retrieved July 29, 2020, from China Satellite Navigation System Management Office Test Evaluation Research Center Test and Assessment Research Center of China Satellite Navigation Office website: http://www.csno-tarc.cn/notice
Diggelen, F. Van. (2020). Google to improve urban GPS accuracy for apps. Retrieved December 9, 2020, from https://www.gpsworld.com
Estey & Wier, S. (2013). "Teqc Tutorial", Basics of Teqc Use and Teqc Products. https://www.unavco.org/software/data-processing/teqc
Groves, P. D. (2015). Principles of GNSS, inertial, and multisensor integrated navigation systems, 2nd edition [Book review]. *IEEE Aerospace and Electronic Systems Magazine*. https://doi.org/10.1109/maes.2014.14110
Guo, F., Zhang, X., & Wang, J. (2015). Timing group delay and differential code bias corrections for BeiDou positioning. *Journal of Geodesy*. https://doi.org/10.1007/s00190-015-0788-2
Hetet, S., & Langley, S. R. B. (2000). Signal-to-Noise Ratio Effects on the Quality of GPS Observations. *Analysis*. http://gauss.gge.unb.ca/papers.pdf/hetet.report.pdf
Kaplan, E. D., & Hegarty, C. J. (2017). Understanding GPS/GNSS: Principles and Applications. In *GNSS Technology and Applications Series*.
Kostelecký, J., Kostelecký, J., & Václavovic, P. (2017). Testing of gnss multipath in different observational conditions at one stationary station. *Acta Geodynamica et Geomaterialia*. https://doi.org/10.13168/AGG.2017.0023
Leick, A., Rapoport, L., & Tatarnikov, D. (2015). GPS Satellite Surveying: Fourth Edition. In *GPS Satellite Surveying: Fourth Edition*. https://doi.org/10.1002/9781119018612
Lu, M., Li, W., Yao, Z., & Cui, X. (2019). Overview of BDS III new signals. *Navigation, Journal of the Institute of Navigation*. https://doi.org/10.1002/navi.296
Luo, X., Lou, Y., Gong, X., Gu, S., & Chen, B. (2018). Benefit of Sparse Reference Network in BDS Single Point Positioning with Single-Frequency Measurements. *Journal of Navigation*. https://doi.org/10.1017/S0373463317000765
Meng, F., Yang, D., Wang, Y., & Zhang, Y. (2018). Study of agricultural machinery operating system based on beidou satellite navigation system. *Advances in Intelligent Systems and Computing*. https://doi.org/10.1007/978-3-319-69096-4_37
Murfin, T. (2020). UAV updates: Overcoming a navigation challenge, autonomous UAS rolls out. Retrieved December 16, 2020, from GPS World website: https://www.gpsworld.com
Pei, T., Pan, W., & Liu, Y. (2017). Research on BDS/GPS dual-mode single point positioning.

Proceedings - 2017 Chinese Automation Congress, CAC 2017, *2017-Janua*, 1163–1168. https://doi.org/10.1109/CAC.2017.8242942

Robustelli, U., Baiocchi, V., & Pugliano, G. (2019). Assessment of dual frequency GNSS observations from a Xiaomi Mi 8 android smartphone and positioning performance analysis. *Electronics (Switzerland)*. https://doi.org/10.3390/electronics8010091

Strode, P. R. R., & Groves, P. D. (2016). GNSS multipath detection using three-frequency signal-to-noise measurements. *GPS Solutions*. https://doi.org/10.1007/s10291-015-0449-1

Vaclavovic, P., & Dousa, J. (2016). G-nut/anubis: Open-source tool for multi-GNSS data monitoring with a multipath detection for new signals, frequencies and constellations. *International Association of Geodesy Symposia*. https://doi.org/10.1007/1345_2015_97

Wen, W. and, & Hsu, L.-T. (2019). Perceived Environment Aided GNSS Single Point Positioning: An Example Using LiDAR Scanner. Retrieved August 13, 2019, from Inside GNSS website: https://insidegnss.com/

XinhuaNet. (2020). China's launch of last BDS satellite draws widespread foreign media coverage. Retrieved December 17, 2020, from XinhuaNet website: http://www.xinhuanet.com/

Yang, Ting, Wan, Wei, Chen, Xiuwan, Chu, Tianxing, Qiao, Zhen, Liang, Hong, Wei, Jiahua, Wang, Guangqian, & Hong, Yang. (2019). Land surface characterization using BeiDou signal-to-noise ratio observations. *GPS Solutions*. https://doi.org/10.1007/s10291-019-0824-4

Yao, Z., Zhang, J., & Lu, M. (2016). ACE-BOC: Dual-frequency constant envelope multiplexing for satellite navigation. *IEEE Transactions on Aerospace and Electronic Systems*. https://doi.org/10.1109/TAES.2015.140607

Ying, W., & Jun, L. (2020). BDS creates more opportunities for global aviation industry. Retrieved December 8, 2020, from People's Daily website: http://en.people.cn/index.html

Zhang, Y., Chen, J., Gong, X., & Chen, Q. (2020). The update of BDS-2 TGD and its impact on positioning. *Advances in Space Research*. https://doi.org/10.1016/j.asr.2020.03.011

Zhao, S., Cui, X., & Lu, M. (2019). Single point positioning using full and fractional pseudorange measurements from GPS and BDS. *Survey Review*. https://doi.org/10.1080/00396265.2019.1683327

BIOGRAPHICAL NOTES

Robert S.B. Galatiya Suya is currently a PhD student at the University of Nottingham Ningbo China (UNNC). He has an MSc in Geodesy and Engineering Surveying from the same university and his research focuses on GNSS multi-frequency algorithm development.

Dr Yung-Tsang Chen obtained his BSc and MSc in Civil Engineering, and PhD in Structural Engineering at University of California, Davis. He currently works as associate professor in Civil Engineering department at the University of Nottingham Ningbo China.

Before joining the University of Nottingham Ningbo China, Dr. C. F. Kwong has at least 19 years of teaching experience in higher education, mostly in the areas of mobile and satellite communications. His research interest includes heterogeneous networks, mobility management for LTE and 5G, and published a number of publications in journal and conferences in this field.

Dr. Kwong is an active member of the IET, having elected as a Chairman of the IET Malaysia Network Young Professional Section from 2008 to 2010 and a committee member of the IET Malaysia Local Network since 2008. His highest position in the IET was being elected as a member of the IET Council for a three-year term from 2011 to 2014. Dr Kwong also a Professional Review Interviewer (PRI) on behalf of the IET, interviewing Chartered Engineer and Incorporated Engineer candidates.

Dr Penghe Zhang obtained his BEng in Civil Engineering, and PhD in Engineering Surveying and Space Geodesy at the University of Nottingham. He currently work as a visiting assistant professor in Civil Engineering department at the University of Nottingham Ningbo China.

Dr Craig Hancock is a Senior Lecturer in Surveying at Loughborough University (UK). Dr Hancock obtained his BSc in Surveying and Mapping Science and his PhD in Space Geodesy from Newcastle University UK. He is a member of the editorial board of the Journal "Survey Review" and is a past Vice Chair of Commission 6 of the FIG.

CONTACTS

Mr. Robert S.B. Galatiya Suya
University of Nottingham Ningbo China, 199 Taikang East Road, Yinzhou District, Ningbo, Zhejiang Province
China.
Email: robert.suya@nottingham.edu.cn

Dr Yung-Tsang Chen
University of Nottingham Ningbo China, 199 Taikang East Road, Yinzhou District, Ningbo, China.
Email: yung-tsang.chen@nottingham.edu.cn
Dr Chiew-Foong Kwong
University of Nottingham Ningbo China, 199 Taikang East Road, Yinzhou District, Ningbo, China
Email: chiew-foong.kwong@nottingham.edu.cn

Dr Penghe Zhang
University of Nottingham Ningbo China, 199 Taikang East Road, Yinzhou District, Ningbo, Zhejiang Province
China.
Email: penghe-zhang@nottingham.edu.cn

Dr Craig Hancock
School of Architecture, Building and Civil Engineering, Loughborough University, Epinal Way, Loughborough, UK, LE11 3TU.
Email: c.m.hancock@lboro.ac.uk